Journal of Applied Polymer Science

REVIEW

Recent Progress in Interfacial Toughening and Damage Self-Healing of Polymer Composites Based on Electrospun and Solution-Blown Nanofibers: An Overview

Xiang-Fa Wu,[1] Alexander L. Yarin[2]

[1]Department of Mechanical Engineering, North Dakota State University, Fargo, North Dakota 58108-6050

[2]Department of Mechanical and Industrial Engineering, University of Illinois at Chicago, Chicago, Illinois 60607-7022

Correspondence to: A. L. Yarin (E-mail: ayarin@uic.edu) or X.-F. Wu (E-mail: xiangfa.wu@ndsu.edu)

ABSTRACT: In this article, we provide an overview of recent progress in toughening and damage self-healing of polymer–matrix composites (PMCs) reinforced with electrospun nanofibers at interfaces with an emphasis on the innovative processing techniques and toughening and damage self-healing characterization. Because of their in-plane fiber architecture and layered structure, high-performance laminated PMCs typically carry low interfacial strengths and interlaminar fracture toughnesses in contrast to their very high in-plane mechanical properties. Delamination is commonly observed in these composite structures. Continuous polymer and polymer-derived carbon nanofibers produced by electrospinning, solution blowing, and other recently developed techniques can be incorporated into the ultrathin resin-rich interlayers (with thicknesses of a few to dozens of micrometers) of these high-performance PMCs to form nanofiber-reinforced interlayers with enhanced interlaminar fracture toughnesses. When incorporated with core–shell healing-agent-loaded nanofibers, these nanofiber-richened interlayers can yield unique interfacial damage self-healing. Recent experimental investigations in these topics are reviewed and compared, and recently developed techniques for the scalable, continuous fabrication of advanced nanofibers for interfacial toughening and damage self-healing of PMCs are given. Developments in the near future in this field are predicted. © 2013 Wiley Periodicals, Inc. J. Appl. Polym. Sci. 130: 2225–2237, 2013

KEYWORDS: composites; electrospinning; fibers; mechanical properties; nanostructured polymers

Received 6 February 2013; accepted 11 March 2013; Published online 10 May 2013

DOI: 10.1002/app.39282

INTRODUCTION

Advanced polymer–matrix composites (PMCs) made of compliant polymeric matrices (typically epoxies) reinforced with high-performance fibers (e.g., high-strength carbon fibers) have emerged as lightweight structural materials of choice for many aerospace and aeronautical applications because of their distinct advantages over traditional metallic materials; these advantages include their highly tailorable anisotropic material properties and related high specific strength and stiffness, excellent formability and manufacturability, and superior immunity to corrosion.[1] Advanced PMCs were first developed for high-value military aircraft and spacecraft in the 1970s by the U.S. Air Force. Today, these advanced composites play a crucial role in a wide range of in-service military aerospace and aeronautical systems and reduce the weight by 10–60% over those based on metal designs; a weight reduction of 20–30% is typical of that achieved by the U.S. Air Force B2 bomber and recent F-22 raptor (24%). With the maturity of composite technologies, we have witnessed a trend of a rapidly expanding adoption of PMCs in commercial transport aviation in past decades. The new Boeing 787 Dreamliner is made from 50 wt % PMCs and more than 50 vol % PMCs. PMCs are also replacing more and more metal parts in ground vehicles and infrastructures as structural agility, fuel efficiency, and material renewability become a worldwide trend and as society also becomes more and more serious about upcoming global challenges, such as the fast depletion of fossil fuel resources and the deterioration of the environment due to the overemission of greenhouse gases and solid wastes.

However, there continue to be barriers and challenges to a more expanded exploitation of composite technologies for primary-transport structures; these include damage tolerance, fuel containment, repair and nondestructive inspection, modeling and failure prediction, and cost-effective manufacturing.[2] Current high-performance structural PMCs carrying highly anisotropic mechanical properties are typically fabricated by means of prepreg-based vacuum bag molding or vacuum-assisted resin-transfer molding (VARTM) techniques. In the latter, in-plane fiber fabrics are commonly used and constitute the reinforcing

framework of the resulting PMCs after resin infusion and curing. The in-plane fiber architecture can benefit extremely from the in-plane uniaxial or biaxial mechanical properties of high-performance laminated PMCs, which can reach those of high-strength steels and alloys. However, compared to their superior in-plane mechanical properties, the out-of-plane properties of advanced PMCs are typically very low; these properties include the interfacial shear strength and interlaminar fracture toughness. Microscopic imaging of the cross sections of advanced PMCs have indicated that there exist ultrathin resin-rich interlayers with thicknesses of a few to dozens of micrometers between neighboring plies (laminas). Such interlayers carry a very low strength and fracture toughness, especially for thermosetting laminated PMCs. In fact, interlaminar fracture (delamination) has commonly been observed in these composite structures, and this has been a focus of research since the birth of advanced laminated composites in the 1970s.[3,4] A variety of toughening techniques have been reported in the literature, specifically aimed at the suppression of the interfacial failure of advanced PMCs; these are reviewed briefly later.

On the other hand, electrospinning as a low-cost, top-down nanofabrication technique has been investigated extensively in the last decade;[5–10] this technique is capable of the scalable production of high-strength, tough continuous polymers and polymer-derived carbon nanofibers (CNFs). These nanofibers can be incorporated into the ultrathin resin-rich interlayers of laminated PMCs to form nanofiber-reinforced interlayers with a high strength and fracture toughness. In addition, when incorporated into core–shell healing-agent-loaded nanofibers, nanofiber-toughened interlayers in laminated PMCs can carry unique interfacial damage self-healing, as we demonstrated recently.[11,12] In this review, we summarize recent experimental investigations on interfacial toughening and damage self-healing techniques based on electrospun nanofibers, particularly for high-performance-fiber (e.g., carbon and glass fibers)-reinforced laminated PMCs. There are two main focuses: (1) the interfacial toughening and damage self-healing mechanisms based on electrospun nanofibers and (2) the high-efficiency, scalable fabrication of continuous core–shell healing-agent-loaded nanofibers by electrospinning and other recently developed low-cost fabrication techniques. The rest of this article consists of the following. In the second section, we present a comparative review of the interfacial failure of laminated PMCs and their conventional toughening techniques. In the third section, we summarize the recent experimental progress in interfacial toughening and damage self-healing of laminated PMCs based on electrospun nanofibers. In the fourth section, we report on the recent progress in core–shell nanofiber fabrication, which is particularly important to the production of continuous core–shell healing-agent-loaded nanofibers uniquely for localized interfacial damage self-healing with low costs and low weight penalties. A brief prospective and concluding remarks on the reviewed topics are contributed in the fifth section.

INTERFACIAL FAILURE OF PMCS AND FAILURE SUPPRESSION TECHNIQUES

Because of the heterogeneous nature of fiber-reinforced laminated PMCs, the stress–strain field and resulting failure process

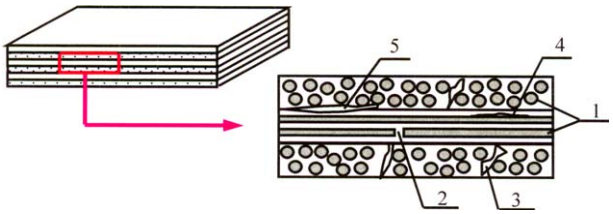

Figure 1. Schematic damage modes in a cross-ply PMC laminate: (1) reinforcing fibers, (2) fiber breakage, (3) matrix cracking, (4) fiber/matrix debonding, and (5) delamination. Reprinted with permission from ref. 12. Courtesy of Wiley Periodicals. [Color figure can be viewed in the online issue, which is available at wileyonlinelibrary.com.]

in laminated PMCs are extremely inhomogeneous. Typically, a locus with the severe stress state may lead to early microdamages (e.g., damage nucleation) in PMCs.[13] The inhomogeneity of the stress–strain field and the randomness of the strength–toughness of composite constituents result in the typical failure process of laminated PMCs, such as a progressive failure of microcrack nucleation, matrix cracking, fiber breakage, fiber and matrix debonding, and delamination.[1,14] The typical damage modes in a cross-ply PMC laminate are illustrated in Figure 1; these include matrix cracking, fiber–matrix debonding, fiber breakage, and delamination. Delamination is a macroscopic failure phenomenon, which is usually the combination of one or several microscopic failure modes. In reality, the damage/failure process in PMCs is much more complicated and is highly dependent on the type of load, fiber, and ply architecture and the physical properties of the constituents. In principle, the strength and toughness of PCMs are the combined effect of the strength and fracture toughness of the constituents (i.e., the reinforcing fibers and polymeric matrix), fiber–matrix interfacial properties (e.g., interfacial physical and chemical properties, roughness), the microstructure of the composite (e.g., fiber alignment, ply layup, volume fraction), dominant failure modes, and stress inhomogeneity (e.g., stress concentration). Given a fiber–matrix combination, a practicable toughening technique, which could enhance the strength and toughness of the resulting PMC system, needs to address one or several dominating factors at an affordable cost.

In the past 4 decades, quite a few effective toughening techniques and concepts have been formulated and implemented in PMCs; these include free-edge-delamination–suppression designs,[1] laminate stitching,[15] modification of matrix resins by incorporation with rigid/rubbery microparticles/nanoparticles,[16,17] controlled fiber debonding and fiber surface treatments,[18] interleaving,[19] and so on. Among these, free-edge-delamination–suppression concepts (e.g., edge reinforcement and edge modification) belong to laminate design at the ply level in altering the singular stress field near the laminate edges;[1–3] this is not closely relevant to materials science, however, but more to accurate free-edge stress analysis.[20] Interleaving is based on the incorporation of discrete thin layers of tough resins, particulates, whiskers, or microfibers into interfaces between neighboring plies of PMCs.[1931–37] The interleaved tough resin (typically thermoplastic epoxy) carries a high shear failure strain and provides enhanced fracture toughness at the

laminate interfaces to suppress delamination. The impact and fatigue damage tolerance of carbon fiber–epoxy laminates can also be noticeably improved[23–26] via the allowance of redundant shear strains along the ply interfaces, which accommodate the strain mismatch across the laminate interfaces. Interleaving has been used in structurally laminated PMCs. However, the thickness of the plastic interleaf is typically comparable to the ply thickness, and this may result in an obvious increase in the laminate thickness and, therefore, a decrease in the unique high specific strength and stiffness of advanced PMCs. Thus, the search for new interfacial toughening techniques with low costs, low weight penalties, and high specific properties of PMCs continues. In addition, all of the previous interfacial toughening techniques do not carry the damage self-healing function. As a matter of fact, the interfacial shear strength and interlaminar fracture toughness of laminated PMCs always degrade with elapsing time, and this has attracted substantial attention of researchers to explore the recent progress in self-healing materials[27–37] for interfacial toughening and damage self-healing of laminated PMCs at low costs and with a low weight penalty.

NANOTECHNOLOGY-BASED INTERFACIAL TOUGHENING TECHNIQUES FOR LAMINATED PMCS

Since the discovery of single-walled crystalline carbon nanotubes (CNTs) in 1991,[38] materials scientists have generally believed that composites made with nanoscale reinforcing materials (e.g., CNTs, platelets, nanoparticles) will carry exceptional mechanical properties superior to those of traditional composites. Although CNTs at a small volume fraction mixed with resins have resulted in remarkable increases in electrical and thermal conductivities triggered by their unique percolation effect, the improvements in the mechanical properties obtained so far are still rather disappointing, particularly when they are compared to those of advanced PMCs reinforced with high-performance continuous fibers.[39–43] Several possible mechanisms have been identified that are responsible for such poor improvements, including inadequate dispersion and alignment of the nanoreinforcing elements, low volume fraction, poor bonding, and insufficient load-transfer properties at the interfaces.[43] In addition, the tensile strengths of CNTs and CNFs may also be much lower than their theoretical predictions because of the unavoidable structural defects induced in the synthesis process and surface doping. So far, despite the extensive research efforts in structural nanocomposites, the prospect of high-strength and high-toughness structural nanocomposites still seems to be remote. However, recent research in nanomanufacturing and nanocomposites has accumulated significant encouraging results in the reinforcement of a small portion of the materials that can be transferred to enhance the mechanical properties of conventional structural PMCs at low cost, low weight penalty, and low impact to the high specific properties of PMCs.[43–50] Among these, interfacial toughening and damage self-healing of PMCs based on electrospun polymers and polymer-derived CNFs have been one of the focuses in the last decade. Substantial experimental works have been performed on controlled nanofiber fabrication, optimal processing of hybrid multiscale composites, and related toughening and damage self-healing characterization.

So far, electrospinning as a low-cost, top-down electrohydrodynamic nanofabrication technique has been used to produce a variety of polymer and polymer-derived nanofibers for broad applications, including nanocomposites, filter media, tissue scaffolds, and so on.[51–55] Recent nanomechanical characterization has indicated that when the diameter is below certain values (from one to a few hundred nanometers), electrospun polymer nanofibers exhibit obviously improved strengths and much higher toughnesses compared to their microfiber and buck counterparts.[56–60] Several potential mechanisms could be responsible for such obvious size effects, and these are still under intensive investigation; these include surface energy, polymer chain alignment, improved crystallinity, and more.[61–64] These low-cost continuous nanofibers provide an excellent nanoreinforcing material for the localized interfacial toughening of PMCs. Among others, Kim and Reneker[65] were the first to produce polymer nanocomposites reinforced with electrospun nanofibers. In their study, chopped electrospun polybenzimidazole (PBI) nanofibers (diameter $\approx$ 300 nm) were used to toughen styrene–butadiene rubber (SBR). Their experiments showed that at a PBI mass ratio of 15%, short PBI nanofiber-toughened SBRs had an average Young's modulus of 19.6 MPa and a tensile strength of 2.8 MPa compared to values of 1.8 and 2.1 MPa, respectively, for the virgin SBR. Nearly a 10-fold modulus improvement and a 70% tensile strength improvement were obtained. Furthermore, Dzenis and Reneker[44] patented the idea of novel delamination-resistant composites prepared by the introduction of small-diameter fibers at ply interfaces, where the electrospun nanofibers were first considered as candidates for interfacial toughening in structurally laminated PMCs [Figure 2(a)].

Furthermore, in his thesis work at the University of Nebraska–Lincoln (Yuris Dzenis's group), Wu[49] conducted systematic studies on the interfacial toughening effect in an aerospace-grade laminated PMC made of unidirectional carbon fiber/epoxy prepregs (Toray P7051S-20Q-F250, Toray America, California) in a wide loading rate from quasistatic and cyclic to dynamic and impact. In the investigation, nonwoven polymer nanofibers [polyacrylonitrile (PAN)] were produced by the electrospinning of about a 10 wt % PAN/*N*,*N*-dimethylformamide (DMF) solution and directly deposited onto the prepreg sheet with a controlled thickness before the laminate panel layup. After vacuum bag molding, the PAN nanofibers were integrated into the resin-rich interlayers to form nanofiber-reinforced interlayers. In quasistatic pure-mode fracture tests based on double-cantilever beam and end-notched flexural specimens, it was found that the PAN nanofibers could enhance the pure-mode fracture toughness by about 30%. A fractographical analysis of the failed samples showed that the toughening mechanisms could include nanofiber pullout, breakage, bridging, and plastic-nanofiber-induced interfacial softening [Figure 1(e,f)].[49] To examine the toughening effect on the edge-delamination strength of laminated PMCs, an angle-ply laminated composite reinforced with nonwoven PAN nanofibers at its interfaces was employed, in which the ply layup was optimized as $[12_2/-12_2/0_2]$ to maximize the out-of-plane shear stress at a given effective axial strain.[20] Although the onset stress for edge delamination

Applied Polymer SCIENCE

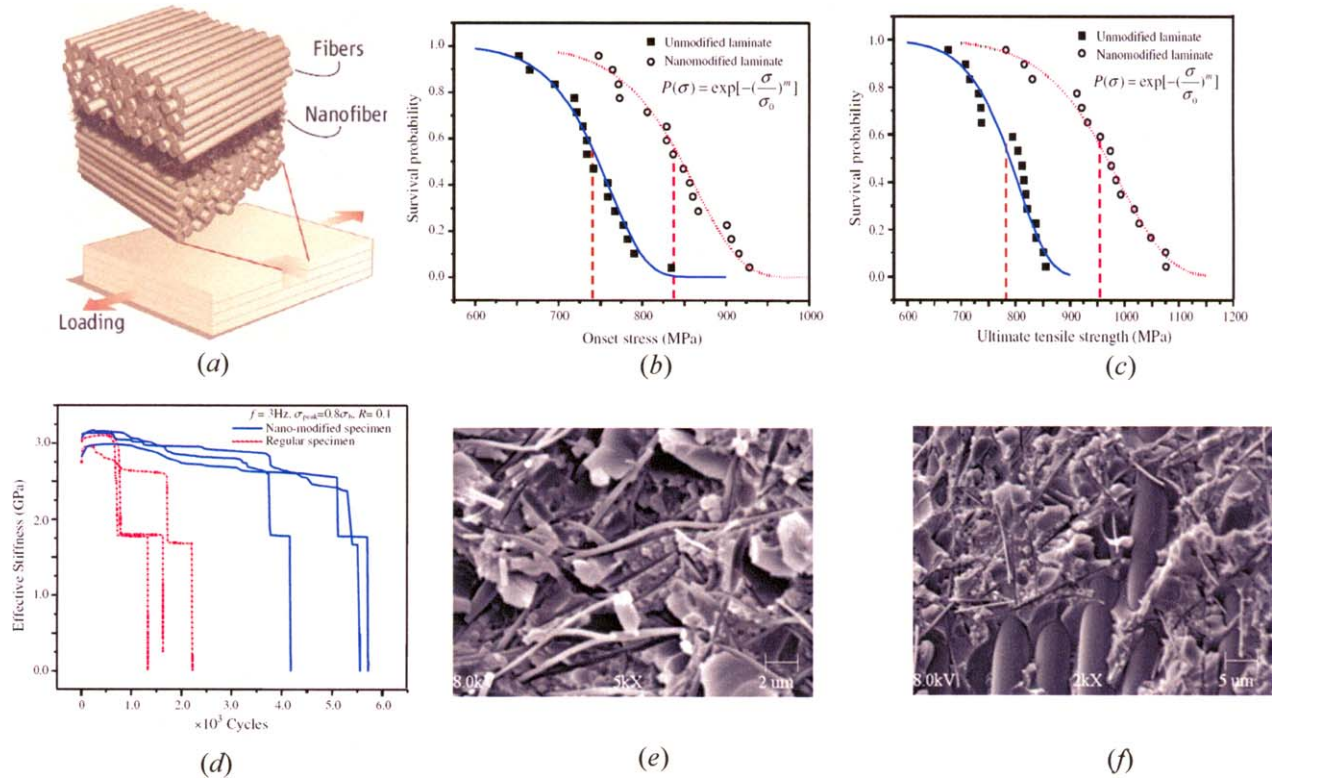

Figure 2. (a) Conceptual hybrid multiscale PMC reinforced with electrospun continuous nanofibers at the interfaces (Reprinted with permission from ref. 43. Copyright 2008 American Association for the Advancement of Science.). (b–d) Toughening effect in edge-delamination onset stress, ultimate toughness strength, and fatigue lifetime of the angle-ply composite laminate with a layup $[12_2/-12_2/0_2]_s$.[49] (e) SEM micrograph of the nanofibers entangled at the ply surface after delamination failure. (f) SEM micrograph of the electrospun nanofibers and reinforcing carbon microfibers entangled at the ply surface after delamination failure. The unidirectional carbon fiber/epoxy prepregs (Toray P7051S-20Q-F250) used in the tests were supplied by Toray America Composites.[49] [Color figure can be viewed in the online issue, which is available at wileyonlinelibrary.com.]

and the ultimate tensile strength of the virgin and nanofiber-toughened specimens were highly scattered, statistical analysis of the experimental data indicated obvious improvements in both the delamination onset stress and the ultimate tensile strength [Figures 2(b,c)]. The unusual increase in the ultimate tensile strength of the tested composite laminate through the addition of a tiny amount of PAN nanofibers (volume fracture <1%) at the 12°/−12° interface was attributed to a plastic softening effect by the plastic nanofibers. Moreover, comparative tension–tension fatigue tests of the same laminated PMCs with and without PAN nanofiber reinforcements indicated that the addition of a tiny amount of plastic PAN nanofibers at the laminate interfaces nearly doubled the cycles of the fatigue lifetime [Figure 2(d)]; this was an exceptional enhancement to the fatigue damage tolerance. Instrumented dynamic fracture tests based on a Hopkinson pressure bar also confirmed the toughening effect of the PAN nanofibers on the dynamic delamination toughness of a thick laminated composite made of 96 unidirectional plies (Toray P7051S-20Q-F250, Toray America).

To extend the previous interfacial toughening method for fiber-reinforced PMCs produced by the low-cost VARTM technique, Fong and coworkers[66–69] recently performed substantial studies of the toughening effect of ultrathin nonwoven CNFs on the interfacial mechanical properties of laminated PMCs. Ultrathin CNF mats were prepared through the electrospinning of PAN nanofibers, and this was followed by thermal treatments, including stabilization at 280°C in air and carbonization at 1200°C in an argon environment.[66] To process the novel hybrid multiscale PMC laminates, the ultrathin CNF mats were first placed on the woven fabric before resin infusion during the VARTM process. After resin infusion and curing, the CNF mats formed toughened interlayers. Three-point flexural and short-beam tests were adopted to evaluate the toughening effect on the out-of-plane mechanical properties of the novel hybrid multiscale composites. The experimental results showed that ultrathin CNF mats at interfaces nearly doubled the interlaminar shear strength, whereas the flexural modulus and work of fracture did not show significant improvements.[66] The authors further considered the toughening effect of CNF mats with different thicknesses and found that the toughening effect could be maximized only at a certain thickness of the CNF layer, which was measured in terms of a nanofiber collecting time around 10 min in their particular experimental setup.[69] In addition, Zhang et al.[70] evaluated the toughening effect of different types of polymer nanofibers on the mode I interlaminar fracture toughness of hybrid multiscale carbon-fiber fabric/epoxy composites with interfaces reinforced with electrospun polymer nanofibers.

Three polymer nanofibers were fabricated and adopted for the evaluations, that is, poly(ε-caprolactone), poly(vinylidene fluoride), and PAN. Their results indicate that poly(vinylidene fluoride) and PAN demonstrated indiscernible toughening effects; however, the poly(ε-caprolactone) nanofibers showed an obvious toughening effect at three different fiber diameters (average), with the improvement as high as 55%, depending on the fiber diameter.

The main advantages of the previous interfacial toughening techniques include the low cost in nanofiber fabrication, low weight penalty to the superior specific strength and stiffness of the PMCs because the toughening nanofibers are highly localized at interfaces, and low impact to the PMC processing such that this interfacial toughening method can be conveniently merged into the conventional PMC process. Thus, this interfacial toughening should have a promising future in PMC industries. However, like all conventional toughening techniques, this nanofiber-based interfacial toughening technique does not carry any damage self-healing function. The interfacial mechanical properties will irreversibly degrade with time. This has recently raised the attention of researcher to resolve this issue.

BIO-INSPIRED INTERFACIAL DAMAGE SELF-HEALING FOR LAMINATED PMCS

In nature, biological bodies have evolved various self-protection functionalities to self-heal damage and function failure (e.g., bleeding, blood clotting, tissue bruising, tree bark compartmentalization healing); this has inspired the development of several damage self-healing mechanisms exploited for use in engineering materials.[35] The exploration of self-healing engineering materials can be tracked to works by Dry and Sottos[71–73] in the early 1990s, where a systematic route was described for achieving self-healing materials.[74] Significant progress in self-healing materials has been made in the last decade after the seminal work on autonomic healing composites based on encapsulated healing agents by White et al.[27] in 2001. Recently, a few comprehensive reviews have been done on the processing of general self-healing materials and composites, damage-healing mechanisms, and related experimental evaluations and modeling.[29,74,75] According to the individual damage-healing mechanisms, self-healing polymeric materials and composites can be classified as follows: (1) self-healing thermoplastic materials based on polymer chain interdiffusion, temperature/photo/UV-induced fusion, and so on, which rely mainly on the high mobility and reactivity of the polymer chains in such materials, and (2) self-healing thermoset materials based on passive mechanical-damage-induced living ring-opening metathesis polymerization (ROMP), in which the healing agent is stored in microcapsules,[27,32,33] hole glass fibers,[35,36] engineered microvascular networks,[76] and so on. In addition, shape-memory polymers and shape-memory polymer/alloy wires have also recently been adopted in self-healing polymeric materials to generate noticeable clamping forces for effective crack closure during the damage-healing process;[77–82] however, external disturbances (e.g., electric current, cooling, heating) are thought to trigger the desired shape-memory effects during the damage-healing process. Thus, additional effort is still needed to incorporate such healing mechanisms into engineered materials and composites within artificial disturbances.

Among these, two such mechanisms based on mammal bleeding strategy have been investigated extensively in recent years. The first is the microencapsulation approach, in which the self-healing system is based on ROMP;[27,32,33] the second is the use of hollow microfibers containing a healing agent with the same ROMP reaction.[35,36] In principle, the microencapsulation approach involves the incorporation of a microencapsulated healing agent and dispersed catalyst particles within the polymeric matrix. Upon cracking, the wax-type microcapsules are ruptured by the propagating crack fronts, and this results in the autonomous release of the healing agent into the crack surfaces through capillary action, as illustrated in Figure 3. The subsequent ROMP of the healing agent (a polymer monomer) triggered by catalyst particles embedded in the matrix heals the material and prevents further crack growth. Dicyclopentadiene (DCPD; $C_{10}H_{12}$) and Grubbs' catalyst have been used broadly as the self-healing system that has been mostly studied for use in PMCs.[83] DCPD is in a liquid state at room temperature and carries a low viscosity; the related ROMP happens rapidly once the Grubbs's catalyst is met, typically in a few seconds to a few minutes, which is suitable for structural damage self-healing.

In addition, damage self-healing mechanisms based on hollow fibers embedded within an engineering material are similar to the arteries in a natural system.[35,36] To incorporate the hollow glass fibers carrying a healing agent into composites, commercially available hollow glass fibers have been demonstrated; they can be directly consolidated into laminas and then manufactured into composite laminates; that is, the self-healing system can also function as a reinforcing element.[35] The key advantages of the hollow fiber self-healing concept are that the fibers can be located to match the orientation of the surrounding reinforcing fibers and thereby minimize the effect of the Poisson's ratio and the mismatch of properties between the self-healing network and the reinforcing fibers. In addition, the fibers can be placed at any location within the stacking sequence to address specific failure threats (Figure 4).

It has been a challenge to directly exploit the previous damage self-healing mechanisms for the interfacial damage self-healing of laminated PMCs because of the large size of the microcapsules and hollow microfibers, which cannot be conveniently integrated into the resin-rich interlayers with their thicknesses of a few to dozens of micrometers. In fact, the relatively large size of the microcapsules (10–1000 μm) may induce additional problems when the microcapsules are integrated into laminated PMCs; these potential problems include the disruption of the fiber architecture (i.e., fiber waviness and fiber volume fraction), the need for a good dispersion of the catalyst to provide uniform healing functionality, microcapsule confinement in a limiting resin volume, and creation of a void in the wake of cracking after the consumption of healing agent.[35] Also, a large volume fraction of microcapsules in the matrix will adversely decrease the unique high specific stiffness and strength of the high-performance PMCs. Additionally, some results have also indicated specific problems in terms of healing efficiency due to the

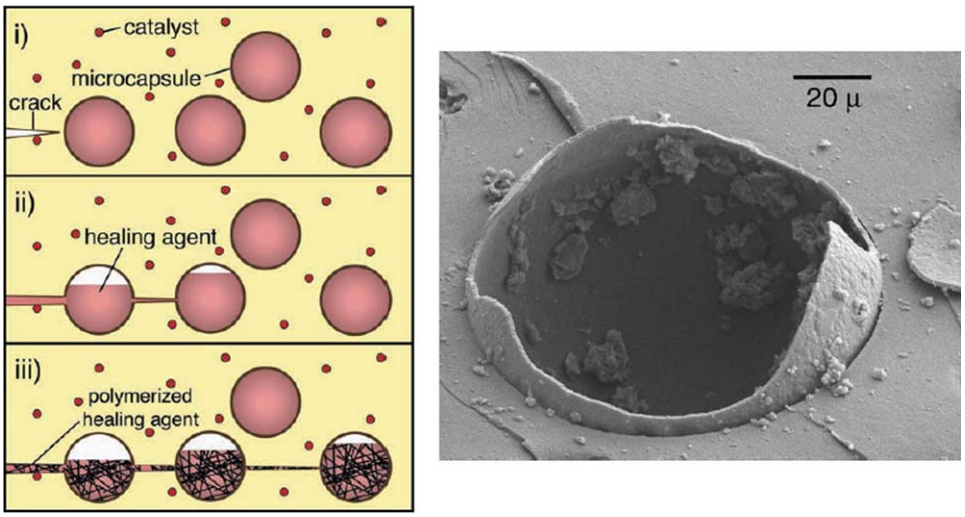

Figure 3. (a) Microencapsulated healing agent embedded in a polymeric matrix containing a catalyst capable of polymerizing the healing agent: (i) cracks formed in the matrix wherever damage occurred; (ii) the crack ruptured the microcapsules, releasing the healing agent into the crack plane through capillary action (the Lucas–Washburn mechanism); and (iii) the healing agent contacted the catalyst triggering polymerization that bound the crack faces closed. (b) SEM image of the fracture plane of a self-healing epoxy with a ruptured urea–formaldehyde microcapsule. Reprinted with permission from ref. 27. Copyright 2001 Macmillan, Ltd. [Color figure can be viewed in the online issue, which is available at wileyonlinelibrary.com.]

clumping of microcapsules into woven–roving wells, where cracks propagate along the woven–roving peaks. Therefore, an optimal damage self-healing strategy is expected to be able to locate and autonomously release healing agent at specific loci of the composites where cracking and damage are most likely to occur, such as at the laminate interfaces.

To resolve this technical challenge, we recently proposed the use of such recently developed fabrication techniques as co-electrospinning, emulsion electrospinning, and solution blowing (see the fourth section) to enwrap the liquid healing agent (e.g., DCPD) into ultrathin polymer nanofibers with the diameter of a couple of micrometers down to hundreds of nanometers.[11,12] As a result, ultrathin nonwoven healing-agent-loaded nanofiber mats can be obtained with tailorable fiber diameters and morphologies through the adjustment the material and process parameters. In one study, wet layup followed by the VARTM technique was used to process hybrid multiscale carbon-fiber/epoxy PMCs (layup: $[0°/\pm45°/90°]$) reinforced with ultrathin healing-agent-loaded core–shell nanofiber mats,[12,84] in which Epon 862 epoxy resin with Epicure 3234 curing agent was selected as the polymeric matrix. It was expected that once delamination occurred, the crack-scissored core–shell nanofibers and liquid healing agent would be autonomously released on the delaminated surface. In the study, a three-point-bending test was adopted to evaluate the damage-healing efficiency of the composite laminate after predamage. The healing efficiency was defined by the flexural stiffness recovery ratio as follows:[12,84]

$$\text{Stiffness recovery ratio} = \frac{\text{Healed flexural stiffness}}{\text{Initial flexural stiffness}} \times 100\% \quad (1)$$

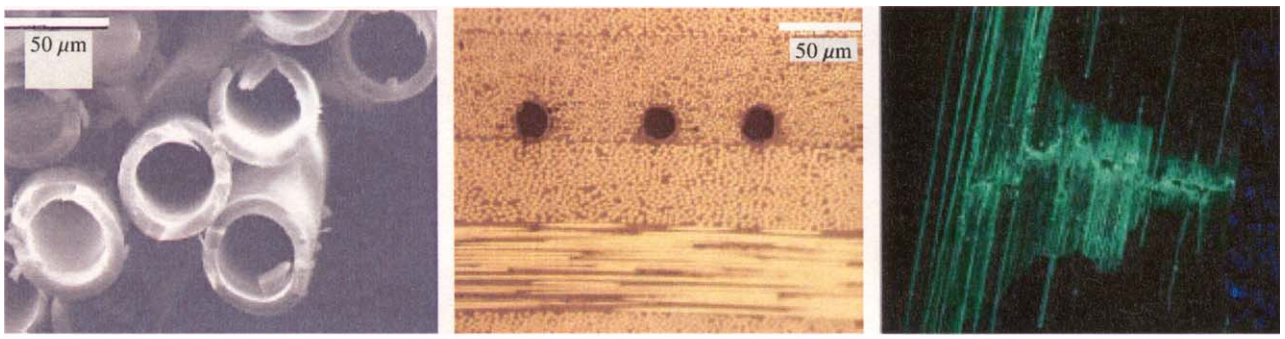

Figure 4. (a) Hollow glass fibers, (b) hollow glass fibers embedded in cross-ply carbon-fiber/epoxy composite laminate, and (c) damage visualization enhancement in a composite laminate by the bleeding mechanism of a fluorescent dye released from hollow glass fibers. Reprinted from ref. 35. Copyright 2007 the Institute of Physics. [Color figure can be viewed in the online issue, which is available at wileyonlinelibrary.com.]

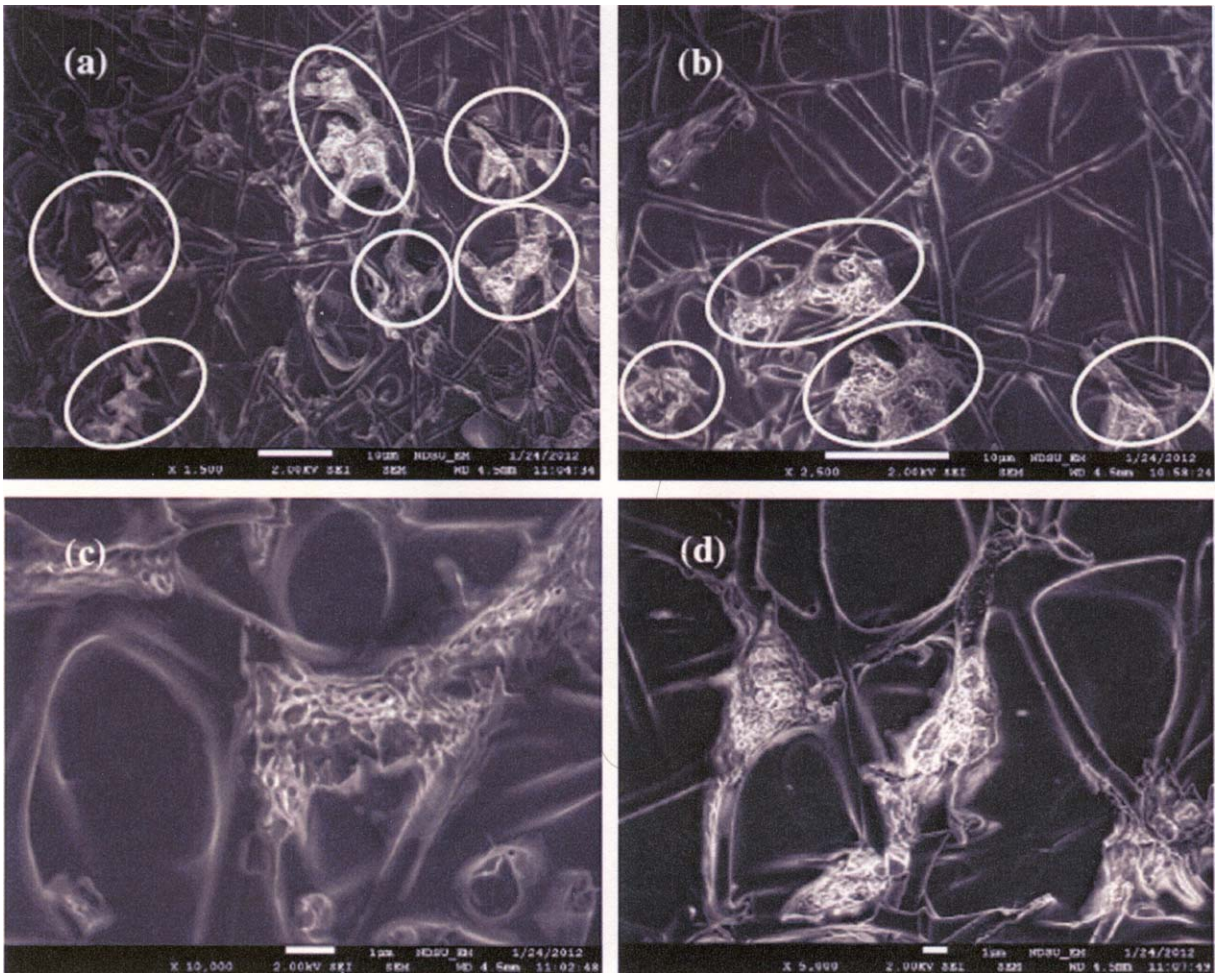

Figure 5. SEM micrographs of the failed surfaces of the hybrid multiscale self-healing PMC after the three-point-bending test (interfacial self-healing mechanisms): (a,b) core–shell nanofiber networks (the circled spots are the regions with autonomously released DCPD after predamage failure) and (c,d) delivery of the healing agent at the core–shell nanofiber breakages due to interfacial and plastic failure of the healed spots after the three-point-bending test.[12,84] Copyright Wiley Periodicals. [Color figure can be viewed in the online issue, which is available at wileyonlinelibrary.com.]

Controlled experiments in the study indicated that after the three-point predamage test, the flexural stiffness was decreased substantially from the original 144.8–163.9 kN/m down to 46.3–61.2 kN/m. After 2 h of damage healing under free-loading conditions, the as-healed stiffness was increased up to 99.0–159.0 kN/m, a nearly 70–100% stiffness recovery.[12,84] Scanning electron microscopy (SEM) based fractographical analysis of the failed surface of the samples indicated the autonomous release of the healing agent (DCPD) at the delaminated surface (Figure 5). After the ROMP reaction, these polymerized DCPDs functioned as discrete pins to bind the delaminated surfaces. In addition, plastic deformation could be clearly differentiated at the healed spots (after final failure), corresponding the substantial shear strains during three-point flexural tests; this allowed significant interfacial strain mismatches particularly popular in laminated PMCs. Similarly, these plastic core–shell nanofibers could also function as toughening nanofibers before scission and similar to the homogeneous toughening nanofibers discussed previously.[12]

Herein, the healing-agent-loaded core–shell nanofibers used for interfacial damage self-healing of laminated PMCs have just started to come into vision. Similar to other self-healing materials and interfacial toughening schemes in laminated PMCs, significant research effects are expected in the near future to determine the fundamentals of the entire process, including the controlled fabrication of healing-agent-loaded core–shell nanofibers, healing-agent delivery, toughening and damage self-healing mechanisms, and optimal design of self-healing laminated PMCs.

HIGH-EFFICIENCY FABRICATION OF CORE–SHELL HEALING-AGENT-LOADED NANOFIBERS

Coaxial electrospinning (co-electrospinning) was developed as a technique allowing the formation of core–shell micrometer-sized fibers and nanofibers with electrified jets of polymer solutions.[85] The physical mechanism of co-electrospinning is similar to that of electrospinning. It is based on the electrically driven bending instability of electrified jets and is a particular example of the Earnshaw's instability in electrostatics.[86,87] The bending instability results in a fractal-like configuration of a polymer jet in flight, and the corresponding enormous length, which it

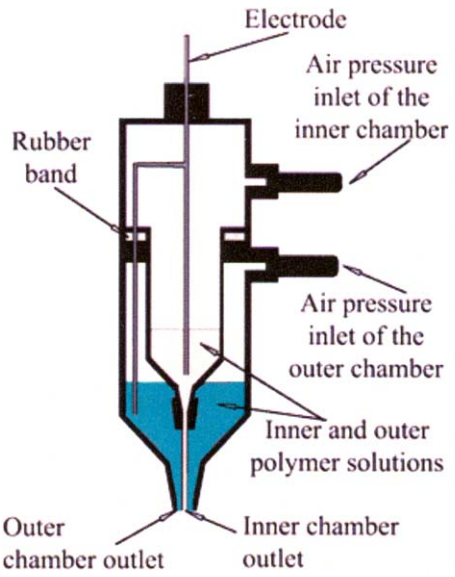

Figure 6. Double-compartment plastic syringe for co-electrospinning. Reprinted with permission from ref. 85. Copyright 2003 John Wiley & Sons. [Color figure can be viewed in the online issue, which is available at wileyonlinelibrary.com.]

acquires at about a 10-cm distance from the needle to the collector. As a result, the jet stretches at the rate on the order of 10^3 s^{-1} and becomes very thin, whereas the viscoelasticity prevents capillary breakup. In parallel, the solvent evaporates, the polymer precipitates and solidifies, and thus, nanofibers are formed.

In co-electrospinning, two polymer solutions are supplied to the core–shell needle separately (Figure 6). At the exit of the core–shell needle attached to the double-compartment syringe emerges a core–shell droplet.[88,89] The droplet is stretched by the electric Maxwell stresses directed toward the counter electrode, and in supercritical regimes when the electric pulling overbears the surface tension and viscoelastic resistance, a core–shell jet is issued from its tip.[90] It is subjected to the bending instability discussed previously. Several reviews have recently devoted been to electrospininning[91–93] and have shown that this technique has been widely used by many research groups.

A simplified version of co-electrospinning, which does not require a core–shell needle, two separate syringe pumps, and pipelines for supplying two polymer solutions, can be realized with a standard electrospinning setup but with its application to Newtonian liquid–polymer or polymer–polymer emulsions.[94] In particular, solutions of poly(methyl methacrylate) (PMMA) and PAN in DMF were blended and left for 1 day to form an emulsion. In 24 h, the blend separated into a 100-μm PMMA/DMF droplet emulsion in a continuous PAN/DMF matrix. This emulsion was electrospun with a standard electrospinning setup [Figure 7(a, left)]. In this case, the core–shell Taylor cone at the needle exit appeared only periodically when a PMMA/DMF droplet was entrained and stuck in the tip of a single-liquid Taylor cone of the PAN/DMF matrix [Figure 7(left)]. Even though the appearance of such stuck PMMA/DMF droplets was intermittent, such droplets existed in most of the process time. An almost 1 m long core was formed from a single droplet, and it was very difficult to find a single-polymer gap between two sections of the core–shell fiber [Figure 7(center)]. The emulsion electrospinning of several other polymers has been described elsewhere.[95–99]

Core–shell fibers formed by emulsion electrospinning have outer diameters in the range 0.5–5 μm; this range is similar to those of fibers formed with co-electrospinning from core–shell needles.[84] To demonstrate the core–shell structure of PMMA/PAN fibers formed by emulsion electrospinning, they are heat-treated to eliminate the PMMA core and carbonize the PAN shell.[82] One resulting carbon tube is shown in the SEM image in Figure 7(right).

A radically different method of forming core–shell nanofibers, so-called solution blowing or emulsion coblowing, was recently introduced for the scalable massive production of core–shell nanofibers.[100–103] This technique employs a high-speed gas flow issued from a high-pressure line at a speed of 200–300 m/s about a core–shell droplet at the needle exit. The droplet can be delivered either from a core–shell needle or from a single needle in the emulsion coblowing case; this is simpler and thus

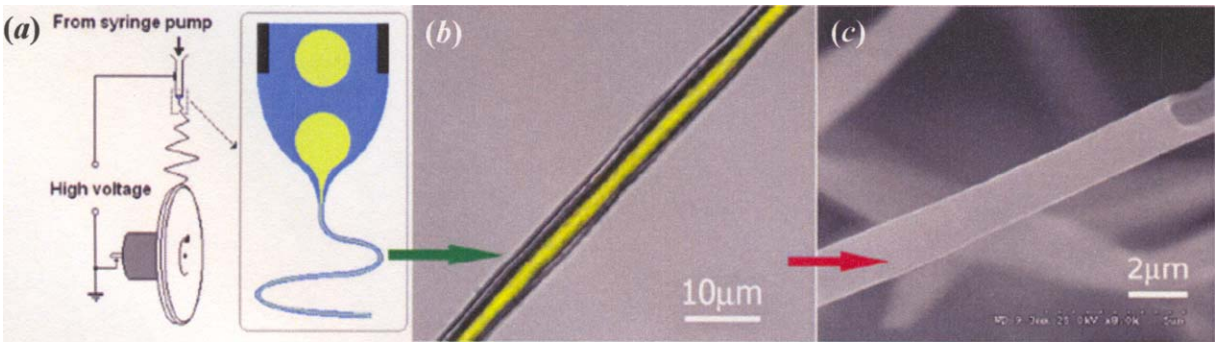

Figure 7. (a) Emulsion electrospinning of the PMMA/PAN blend in DMF with a single needle.[94] The inset (on the left) shows a magnified detail of the needle orifice; this is shown by two parallel black lines on top. The PMMA/DMF droplets are shown in yellow and the PAN/DMF matrix is shown in blue in the online figure. In this case, the core–shell fibers could be collected either on a plane counter electrode or on the edge of a rotary disk serving as a grounded electrode, as shown in the sketch. (b,c) Optical image of a core–shell microfiber collected on a glass slide that was placed between the electrodes. The fiber was not fully stretched yet because it was intercepted in flight by the glass slide. Reprinted from ref. 94. Copyright 2007 American Chemical Society. [Color figure can be viewed in the online issue, which is available at wileyonlinelibrary.com.]

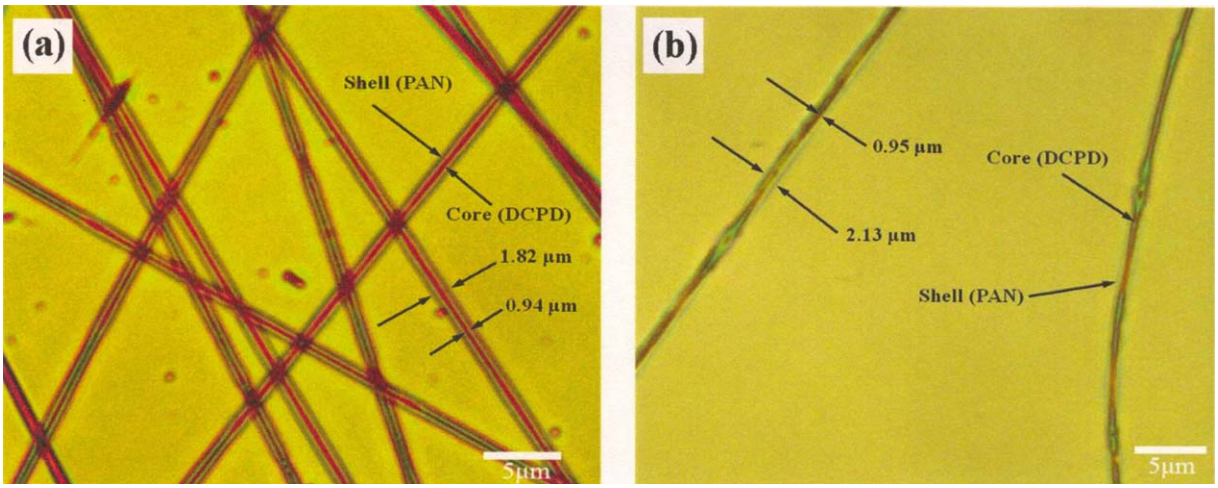

Figure 8. Optical images of the co-electrospun core–shell DCPD/PAN nanofibers.[11] Panel (a) shows relatively uniform nanofibers, whereas panel (b) depicts nanofibers affected by capillary instability visible as a series of undulations. The scale bar in both images is 5 μm. Reprinted from ref. 11. Copyright 2012 Royal Society of Chemistry. [Color figure can be viewed in the online issue, which is available at wileyonlinelibrary.com.]

preferable. The droplet driven by the gas jet stretches and issues a core–shell jet from its tip. The latter is stretching and bending vigorously under the action of the gas flow as a result of the aerodynamically driven bending instability.[104,105] The jet cross-sectional diameter rapidly reduces to the nanoscale, which after the solvent evaporates, results in nanofibers. The productivity of

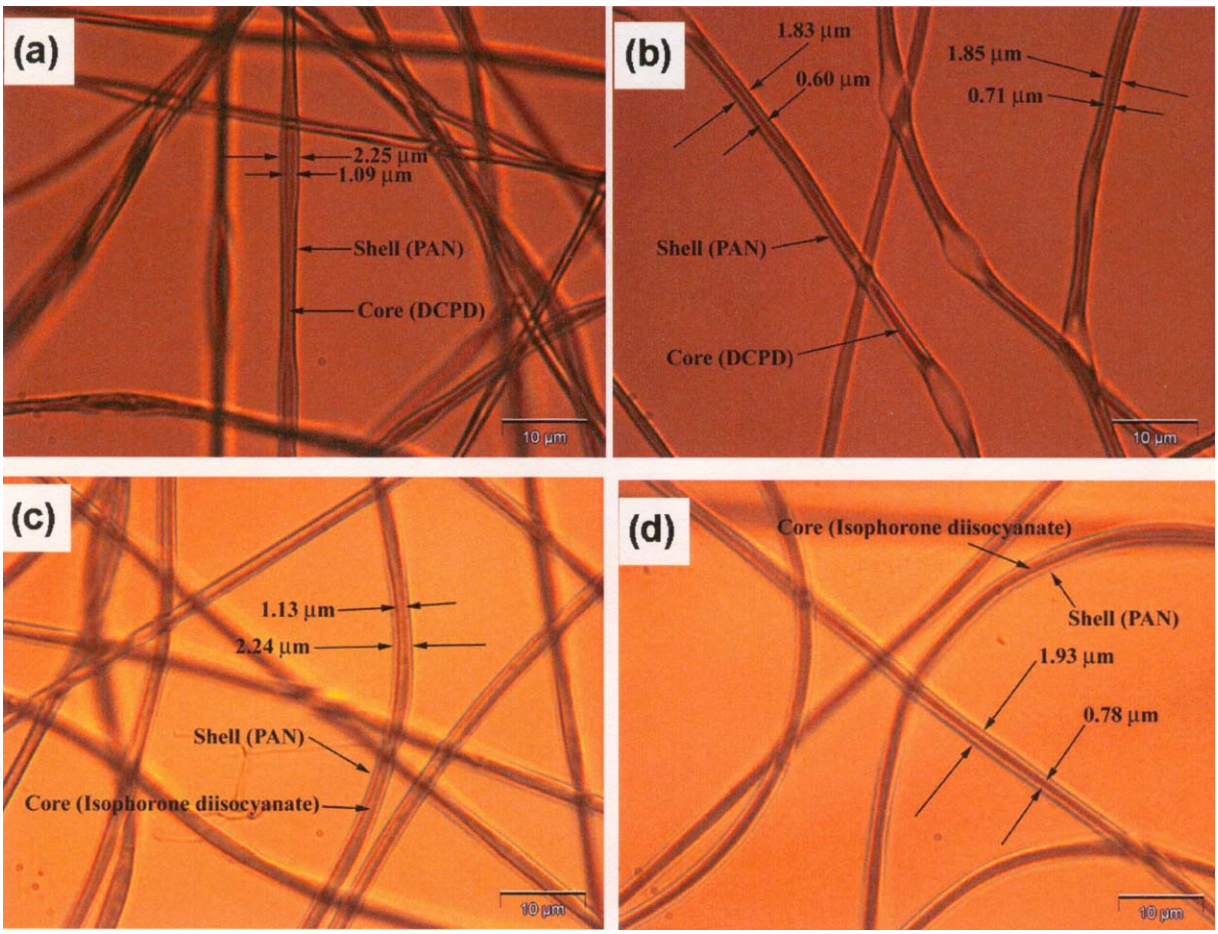

Figure 9. Optical images of the core–shell emulsion–electrospun fibers.[11] (a,b) Core–shell fibers formed from the emulsion of DCPD in PAN and DMF with DCPD eventually occupying the core and PAN (the shell). (c,d) Core–shell fibers formed from the emulsion of PAN and IPDI in DMF, with PAN eventually occupying the shell and the IPDI (the core). The scale bar in all of the images is 10 μm. Reprinted from ref. 11. Copyright 2012 Royal Society of Chemistry. [Color figure can be viewed in the online issue, which is available at wileyonlinelibrary.com.]

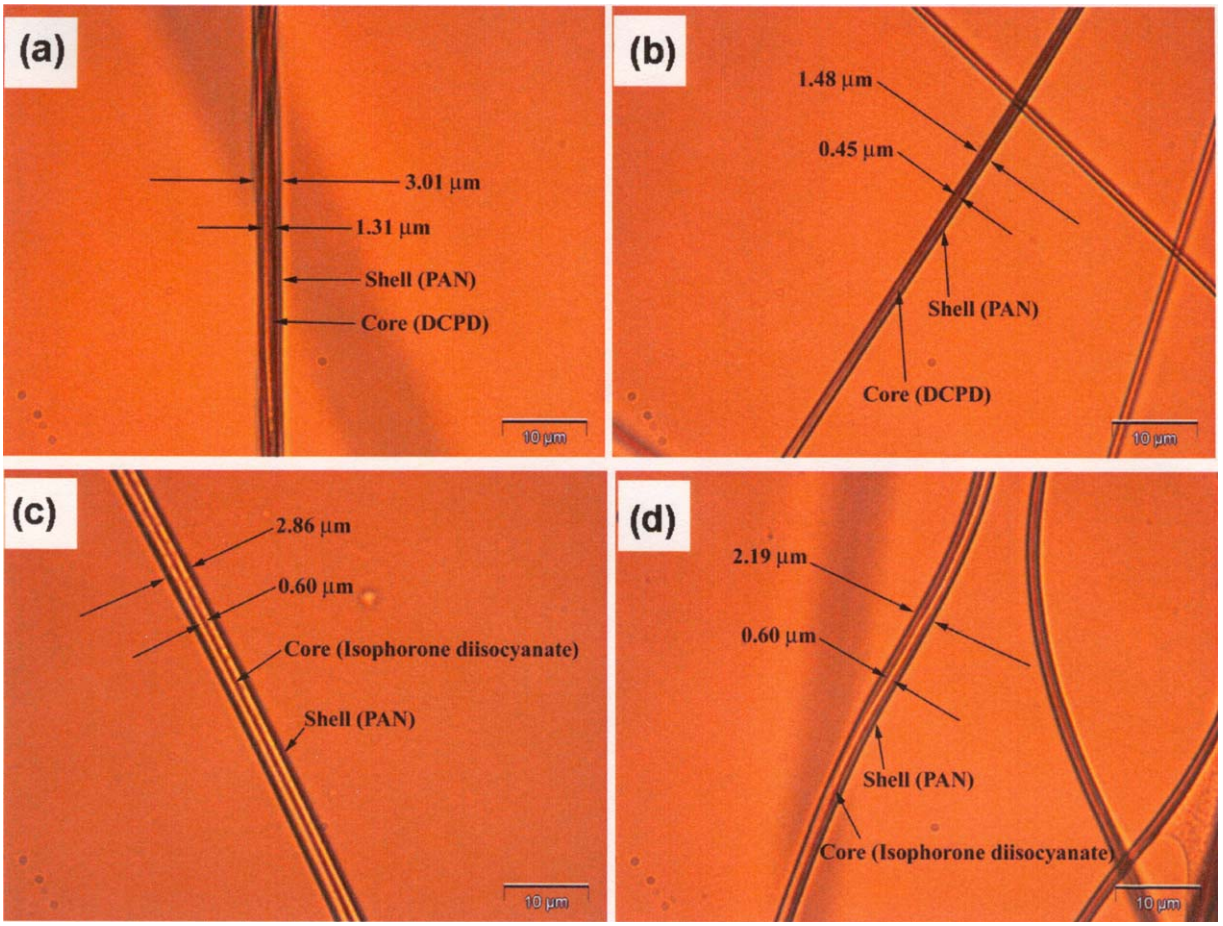

Figure 10. Optical images of the core–shell fibers formed with the emulsion solution coblowing.[11] (a,b) Core–shell fibers obtained from the emulsion of DCPD in PAN and DMF. In these core–shell fibers, DCPD occupied the core, and PAN occupied the shell. (c,d) Core–shell fibers formed from the emulsion of PAN and IPDI in DMF. In these fibers, IPDI occupied the core, whereas PAN was in the shell. The scale bar in all of the images is 10 μm. Reprinted from ref. 11. Copyright 2012 Royal Society of Chemistry. [Color figure can be viewed in the online issue, which is available at wileyonlinelibrary.com.]

the emulsion coblowing method is at least 10 times higher than that of co-electrospinning and emulsion electrospinning.

On the basis of the three methods described previously (co-electrospinning, emulsion electrospinning, and solution blowing), we recently encapsulated the liquid healing agents [in particular, DCPD and isophorone diisocyanate (IPDI)] into ultrathin polymer fibers with outer diameters in the range from 100 nm to several micrometers.[11,12]

Figure 8 depicts the core–shell PAN/DCPD nanofibers formed with co-electrospinning from a core–shell needle. It was shown [Figure 8(a)] that liquid DCPD dissolved in DMF was encapsulated in the core surrounded by the outer PAN shell. Such core–shell DCPD/PAN nanofibers hold great promise for damage self-healing purposes in ultrathin geometries. The image in Figure 8(b) shows that the fiber capillary instability of the fiber surface and core were occasionally observed under the improper conditions of the co-electrospinning, in particular, with too-dilute solutions.

The microfibers formed by the emulsion electrospinning are shown in Figure 9. These electrospun core–shell fibers were formed from an emulsion of 8 wt % PAN and 5 wt % DCPD. They were collected on a glass slide and observed under an optical microscope [Figures 9(a,b)]. Figure 9(b) shows that some fibers were slightly beaded; this was probably caused by the onset of capillary instability. In the case of the emulsion electrospun fibers, the core diameter was approximately in the range 0.4–1.5 μm; the shell diameter was in the range 1.5–3 μm. The emulsion electrospinning of 8 wt % PAN and 5 wt % IPDI in DMF was also possible.[11] Such core–shell fibers were highly uniform [Figures 9(c,d)]. They had core diameters in the range 0.51–2.01 μm and shell diameters in the range 1.75–3.81 μm.

The emulsions used in emulsion electrospinning were also tested in emulsion solution coblowing.[11] The solution-blown fibers collected on glass slides and were inspected under an optical microscope. The optical images of the core–shell fibers blown from the DCPD/PAN emulsions in DMF and those from the IPDI/PAN emulsions in DMF are shown in Figures 10(a,b) and 10(c,d), respectively. Figures 10(a,b) show that in the solution-blown DCPD/PAN fibers, the shell diameter (PAN) ranged from approximately 1.35 to 3.00 μm, whereas the DCPD core diameter was in the range from 0.44 to 1.30 μm. For

comparison, in the solution-blown IPDI/PAN fibers shown in Figures 10(c,d), the shell diameter (PAN) ranged from 1.80 to 2.90 μm, whereas the core diameter (IPDI) was in the range 0.40–0.95 μm.

PROSPECTIVE AND CONCLUDING REMARKS

The tough homogeneous nanofibers and core–shell healing-agent-loaded nanofibers produced by co-electrospinning, solution blowing, and several other advanced nanofabrication techniques reviewed in this article provide a new horizon for the use of low-cost continuous nanofibers for interfacial toughening and damage self-repairing of high-value advanced structural composites. New research is still expected to elucidate the toughening and damage self-healing mechanisms of such nanofiber-integrated ultrathin interlayers embedded in polymer composites for the purpose of controlled fabrication and rational modeling.

In addition, the three most recently developed nanofabrication methods for producing core–shell nanofibers (co-electrospinning, emulsion electrospinning, and emulsion solution coblowing) have been comparatively reviewed and were shown to be fully capable of fabricating core–shell fibers with several healing agents (DCPD or IPDI) encapsulated in the core. The core in these fibers is surrounded by a polymer shell, which provides them with structural stability. Even though the fiber sizes and quality are approximately the same in all of these methods, the productivity that is highly important to scale-up is incomparably higher in the solution coblowing method, and this probably makes it preferable for mass production.

An important question associated with self-healing core–shell fibers is related to their expected rate of healing. Even though the linear scales involved are on the order of several hundred nanometers to a few micrometers, the flow and curing rates of highly viscous healing agents under the conditions of the low Reynolds number and creeping flows might be quite significant. Therefore, one probably cannot expect an instantaneous healing but rather a slow but persistent healing of arising microcracks. A detailed exploration of the experimental and theoretical aspects of such healing processes and the accompanying preservation or recovery of material strength are attractive and important directions for the future research.

Consequently, the research in this topic would greatly advance the fundamental understanding of interfacial engineering in polymer composites and controllable nanomanufacturing for the mass production of nanofibers. Research activities in interfacial toughening and damage self-healing would greatly benefit new generations of high-strength, high-toughness structural polymer composites with damage self-healing functions and other advanced composites with nanoengineered multifunctional interfaces.

REFERENCES

1. Jones, R. M. Mechanics of Composite Materials, 2nd ed.; Taylor & Francis: Philadelphia, **1999**.
2. Tenney, D.; Pipes, R. B. Presented at the 7th Japan International SAMPE Symposium and Exhibition, Tokyo, Japan, **2001**.
3. Pipes, R. B.; Pagano, N. J. J. *Compos. Mater.* **1970**, *4*, 538.
4. Pipes, R. B.; Daniel, I. M. J. *Compos. Mater.* **1971**, *5*, 255,
5. Doshi, J.; Reneker, D. H. J. *Electrostat.* **1995**, *35*, 151.
6. Reneker, D. H.; Chun, I. *Nanotechnology* **1996**, *7*, 216.
7. Dzenis, Y. *Science* **2004**, *304*, 1917.
8. Reneker, D. H.; Yarin, A. L.; Zussman, E.; Xu, H. *Adv. Appl. Mech.* **2007**, *41*, 43.
9. Reneker, D. H.; Yarin, A. L. *Polymer* **2008**, *49*, 2387.
10. Greiner, A.; Wendorff, J. H. *Angew. Chem. Int. Ed.* **2007**, *46*, 5670.
11. Sinha-Ray, S.; Pelot, D. D.; Zhou, Z. P.; Rahman, A.; Wu, X. F.; Yarin, A. L. J. *Mater. Chem.* **2012**, *22*, 9138.
12. Wu, X. F.; Rahman, A.; Zhou, Z. P.; Pelot, D. D.; Sinha-Ray, S.; Chen, B.; Payne, S.; Yarin, A. L. J. *Appl. Polym. Sci.*, to appear.
13. Gdoutos, E. E.; Pilakoutas, K.; Rodopoulos, C. A. Failure Analysis of Industrial Composite Materials; McGraw-Hill: New York, **2000**.
14. Tarpani, J. R.; Bose, W. W.; Spinelli, D. *Mater. Res.* **2006**, *9*, 115.
15. Dransfield, K.; Baillie, C.; Mai, Y. W. *Compos. Sci. Tech.* **1994**, *50*, 305.
16. Garg, A. C.; Mai, Y. W. *Compos. Sci. Tech.* **1998**, *31*, 179.
17. Low, I. M.; Mai, Y. M. In Handbook of Ceramics and Composites; Cheremisinoff, N. P., Ed.; CRC: Boca Raton, **1990**; Vol. *2*, p 105.
18. Kim, J. K.; Mai, Y. W. *Compos. Sci. Tech.* **1991**, *41*, 333.
19. Carlsson, L. A.; Aksoy, A. *Int. J. Fracture* **1999**, *52*, 67.
20. Wu, X. F.; Dzenis, Y. A. *Compos. Struct.* **2005**, *70*, 100.
21. Carlsson, L. A. *Key Eng. Mater.* **1996**, *121–122*, 489
22. Xu, L. Y. J. *Compos. Mater.* **1994**, *13*, 509.
23. Ogihara, S.; Takeda, N.; Kobayashi, S.; Kobayashi, A. *Compos. Sci. Tech.* **1999**, *59*, 1387.
24. Ogihara, S.; Takeda, N.; Kobayashi, S.; Kobayashi, A. *Int. J. Fatigue* **2002**, *24*, 93.
25. Takeda, N.; Kobayashi, S.; Ogihara, S.; Kobayashi, A. *Int. J. Fatigue* **1999**, *21*, 235.
26. Walker, L.; Sohn, M. S.; Hu, X. Z. *Compos. A* **2002**, *33*, 893.
27. White, S. R.; Sottos, N. R.; Moore, J.; Geubelle, P.; Kessler, M.; Brown, E.; Suresh, S.; Viswanathan, S. *Nature* **2001**, *409*, 794.
28. Wool, R. P. *Nature* **2001**, *409*, 794.
29. Wu, D. Y.; Meure, S. M.; Soloman, D. *Prog. Polym. Sci.* **2008**, *33*, 479.
30. van der Zwaag, S. Self-Healing Materials—An Alternative Approach to 20 Centuries of Materials Science. Springer: Dordrecht, The Netherlands, **2007**.
31. Ghosh, S. K. Self-Healing Materials: Fundamentals, Design Strategies, and Applications; Wiley-VCH: Weinheim, Germany, **2009**.
32. Kessler, M. R.; Sottos, N. R.; White, S. R. *Compos. A* **2003**, *34*, 743.
33. Sottos, N. R.; White, S. R.; Bound, I. J. R. *Soc. Interface* **2007**, *4*, 347.

34. Hayes, S. A.; Jones, F. R.; Marshiya, K.; Zhang, W. *Compos. A* **2007**, *38*, 1116.
35. Trask, R. S.; Williams, G. J.; Bond, I. P. *Bioinsp. Biomim.* **2007**, *2*, 1.
36. Trask, R. S.; Williams, G. J.; Bond, I. P. J. *R. Soc. Interface* **2007**, *4*, 363.
37. Yin, T.; Rong, M. Z.; Wu, J.; Chen, H.; Zhang, M. Q. *Compos. A* **2008**, *39*, 1479.
38. Iijima, S. *Nature* **1991**, *354*, 56.
39. Thostenson, E. T.; Li, C. Y.; Chou, T. W. *Compos. Sci. Tech.* **2005**, *65*, 471.
40. Coleman, J. N.; Khan, U.; Gun'ko, Y. K. *Adv. Mater.* **2006**, *18*, 689.
41. Njuguna, J.; Pielichowski, K.; Alcock, J. R. *Adv. Eng. Mater.* **2007**, *9*, 835.
42. Alexandre, M.; Dubois, P. *Mater. Sci. Eng. R.* **2000**, *28*, 1.
43. Dzenis, Y. *Science* **2008**, *319*, 419.
44. Dzenis, Y. A.; Reneker, D. H. U.S. Pat. 6,265,333 (**2001**).
45. Thostenson, E. T.; Li, W. Z.; Wang, D. Z.; Ren, Z. F.; Chou, T. W. J. *Appl. Phys.* **2002**, *91*, 6034.
46. Veedu, V. P.; Cao, A.; Li, X. S.; Ma, K. G.; Soldano, C.; Kar., S.; Ajayan, P. M.; Ghasemi-Nejhad, M. N. *Nat. Mater.* **2006**, *5*, 457.
47. Bekyarova, E.; Thostenson, E. T.; Yu, A.; Kim, H.; Gao, J.; Tang, J.; Hahn, H. T.; Chou, T. W.; Itkis, M. E.; Haddon, R. C. *Langmuir* **2007**, *23*, 3970.
48. Thostenson, E. T.; Yu, A.; Itkis, M. E.; Fakhrutdinvo, D.; Chou, T. W.; Haddon, R. C. J. *Phys. Chem.* **2007**, *111*, 17865.
49. Wu, X. F. Ph.D. Thesis, University of Nebraska–Lincoln, **2003**.
50. Chou, T. W.; Gao, L. M.; Thostenson, E. T.; Zhang, Z. G.; Byun, J. H. *Compos. Sci. Technol.* **2010**, *70*, 1.
51. Huang, Z. M.; Zhang, Y. Z.; Kotaki, M.; Ramakrishna, S. *Compos. Sci. Technol.* **2003**, *63*, 2223.
52. Chronakis, I. S. J. *Mater. Process. Tech.* **2005**, *167*, 283.
53. Li, D.; Xia, Y. N. *Adv. Mater.* **2004**, *16*, 1151.
54. Ramaseshan, R.; Sundarrajan, S.; Jose, R.; Ramakrishna, S. J. *Appl. Phys.* **2007**, *102*, 111101.
55. Baji, A.; Mai, Y. W.; Wong, S. C.; Abtahi, M.; Chen, P. *Compos. Sci. Technol.* **2010**, *70*, 703.
56. Tan, E. P. S.; Lim, C. T. *Rev. Sci. Instrum.* **2004**, *75*, 2581.
57. Tan, E. P. S.; Goh, C. N.; Sow, C. H.; Lim, C. T. *Appl. Phys. Lett.* **2005**, *86*, 073115.
58. Zussman, E.; Burman, M.; Yarin, A. L.; Khalfin, R.; Cohen, Y. J. *Polym. Sci. Part B: Polym. Phys.* **2006**, *44*, 1482.
59. Naraghi, M.; Chasiotis, I.; Kahn, H.; Wen, Y. K.; Dzenis, Y. *Appl. Phys. Lett.* **2007**, *91*, 151901.
60. Naraghi, M.; Chasiotis, I.; Kahn, H.; Wen, Y.; Dzenis, Y. *Rev. Sci. Instrum.* **2006**, *78*, 085108.
61. Arinstein, A.; Burman, M.; Gendelman, O.; Zussman, E. *Nat. Nanotechnol.* **2007**, *2*, 59.
62. Wu, X. F.; Kostogorova-Beller, Y. Y.; Goponenko, A. V.; Hou, H. Q.; Dzenis, Y. A. *Phys. Rev. E* **2008**, *78*, 061804.
63. Wu, X. F.; Dzenis, Y. A. J. *Appl. Phys.* **2007**, *102*, 044306.
64. Wu, X. F. J. *Appl. Phys.* **2010**, *107*, 013509.
65. Kim, J. S.; Reneker, D. H. *Polym. Compos.* **1999**, *20*, 124.
66. Chen, Q.; Zhang, L. F.; Yoon, M. K.; Wu, X. F.; Arefin, R. H.; Fong, H. J. *Appl. Polym. Sci.* **2012**, *124*, 444.
67. Chen, Q.; Zhang, L. F.; Rahman, A.; Zhou, Z. P.; Wu, X. F.; Fong, H. *Compos. A* **2011**, *42*, 2036.
68. Chen, Q.; Zhang, L. F.; Zhao, Y.; Wu, X. F.; Fong, H. *Compos. B* **2012**, *43*, 309.
69. Chen, Q.; Zhao, Y.; Zhou, Z. P.; Rahman, A.; Wu, X. F.; Wu, W. D.; Xu, T.; Fong, H. *Compos. B* **2013**, *44*, 1.
70. Zhang, J.; Yang, T.; Lin, T.; Wang, C. H. *Compos. Sci. Tech.* **2012**, *72*, 256.
71. Dry, C. M. *MRS Proc.* **1992**, *276*, 311.
72. Dry, C. M. *SPIE Proc.* **1992**, *1777*, 367.
73. Dry, C. M.; Sottos, N. *SPIE Proc.* **1993**, *1916*, 438.
74. Wool, R. P. *Soft Matter* **2008**, *4*, 400.
75. Murphy, E. B.; Wudl, F. *Prog. Polym. Sci.* **2010**, *35*, 223.
76. Toohey, K. S.; Sottos, N. R.; Lewis, J. A.; Moore, J. S.; White, S. R. *Nat. Mater.* **2007**, *6*, 518.
77. Kirkby, E. L.; Rule, J. D.; Michaud, V. J.; Sottos, N. R.; White, S. R.; Månson, J. A. E. *Adv. Funct. Mater.* **2008**, *18*, 2253.
78. Kirkby, E. L.; Michaud, V. J.; Månson, J. A. E.; Sottos, N. R.; White, S. R. *Polymer* **2009**, *50*, 5533.
79. Nji, J.; Li, G. *Polymer* **2010**, *51*, 6021.
80. Li, G.; Meng, H.; Hu, J. J. R. *Soc. Interface* **2012**, *9*, 3279.
81. Neuser, S.; Michaud, V.; White, S. R. *Polymer* **2012**, *53*, 370.
82. Li, G.; Ajisafe, O.; Meng, H. *Polymer* **2013**, *54*, 920.
83. Bielawski, C. W.; Grubbs, R. H. *Prog. Polym. Sci.* **2007**, *32*, 1.
84. Rahman, A. M. S. Thesis, North Dakota State University, **2012**.
85. Sun, Z.; Zussman, E.; Yarin, A. L.; Wendorff, J. H.; Greiner, A. *Adv. Mater.* **2003**, *15*, 1929.
86. Reneker, D. H.; Yarin, A. L.; Fong, H.; Koombhongse, S. J. *Appl. Phys.* **2000**, *87*, 4531.
87. Jeans, J. The Mathematical Theory of Electricity and Magnetism; Cambridge University Press: Cambridge, United Kingdom, **1958**.
88. Zussman, E.; Yarin, A. L.; Bazilevsky, A. V.; Avrahami, R.; Feldman, M. *Adv. Mater.* **2006**, *18*, 348.
89. Reznik, S. N.; Yarin, A. L.; Zussman, E.; Bercovici, L. *Phys. Fluids* **2006**, *18*, 062101.
90. Han, T.; Yarin, A. L.; Reneker, D. H. *Polymer* **2008**, *49*, 1651.
91. Greiner, A.; Wendorff, J. H.; Yarin, A. L.; Zussman, E. *Appl. Microbiol. Biotech.* **2006**, *71*, 387.
92. Yarin, A. L.; Zussman, E.; Wendorff, J. H.; Greiner, A. J. *Mater. Chem.* **2007**, *17*, 2585.
93. Yarin, A. L. *Polym. Adv. Technol.* **2011**, *22*, 310.

94. Bazilevsky, A. V.; Yarin, A. L.; Megaridis, C. M. *Langmuir* **2007**, *23*, 2311.

95. Li, X. H.; Shao, C. L.; Liu, Y. C. *Langmuir* **2007**, *23*, 10920.

96. Kim, C.; Jeong, Y. I.; Ngoc, B. T. N.; Yang, K. S.; Kojima, M.; Kim, Y. A.; Endo, M.; Lee, J. W. *Small* **2007**, *3*, 91.

97. Zhang, J. F.; Yang, D. Z.; Xu, F.; Zhang, Z. P.; Yin, R. X.; Nie, J. *Macromolecules* **2009**, *42*, 5278.

98. Angeles, M.; Cheng, H. L.; Velankar, S. S. *Polym. Adv. Technol.* **2008**, *19*, 728.

99. Xu, X. L.; Zhuang, X. L.; Chen, X. S.; Wang, X.; Yang, L.; Jing, X. *Macromol. Rapid Commun.* **2006**, *27*, 1637.

100. Sinha-Ray, S.; Yarin, A. L.; Pourdeyhimi, B. *Carbon* **2010**, *48*, 3575.

101. Sinha-Ray, S.; Zhang, Y.; Yarin, A. L.; Davis, S. C.; Pourdeyhimi, B. *Biomacromolecules* **2011**, *12*, 2357.

102. Khansari, S.; Sinha-Ray, S.; Yarin, A. L.; Pourdeyhimi, B. J. *Appl. Phys.* **2012**, *111*, 044906.

103. Khansari, S.; Sinha-Ray, S.; Yarin, A. L.; Pourdeyhimi, B. *Ind. Eng. Chem. Res.* **2012**, *51*, 15109.

104. Sinha-Ray, S.; Yarin, A. L.; Pourdeyhimi, B. J. *Appl. Phys.* **2010**, *108*, 034912.

105. Yarin, A. L.; Sinha-Ray, S.; Pourdeyhimi, B. J. *Appl. Phys.* **2010**, *108*, 034913.